Numerical Analysis and Optimization of a Multi-Mode Interference Based Polarization Beam Splitter

Yannick D'Mello*[1], James Skoric[1], Eslam Elfiky[1], Michael Hui[1], David Patel[1], Yun Wang[1], and David Plant[1]
1. Department of Electrical and Computer Engineering, McGill University, Montreal, Canada
*Yannick.DMello@mail.McGill.ca

The demand for photonic devices is increasingly pushing towards smaller size and higher efficiency. Silicon-on-Insulator (SOI) is a promising platform for photonic circuits due to its high refractive index and compatibility with complementary metal-oxide-semiconductor (CMOS) technology. However, the inherent birefringence in SOI devices implies that they are sensitive to polarization, which introduces the need for polarization discrimination and conversion through devices such as rotators or splitters. These devices have become essential to the development of SOI based photonic circuits. This paper reports the development and characterization of an on-chip polarization splitter that is limited in geometric complexity so as to ensure its tolerance to fabrication variations. The splitter demonstrates an insertion loss of 0.82 dB for the TE_0 mode and 1.56 dB for the TM_0 mode over the telecommunication C-band wavelength range.

Keywords: Silicon photonics, polarization beam splitter, multi-mode interferometer, COMSOL Wave Optics, telecommunications.

I. Introduction

The progression toward smaller and faster photonic circuits has led to the development of nanophotonic platforms that facilitate the fabrication of multiple devices onto a single integrated chip. The Silicon Photonics (SiP) platform leverages Complementary Metal-Oxide-Semiconductor (CMOS) technology to develop inexpensive, robust, and mass-manufacturable Silicon Electronic-Photonic Integrated Circuits (SiEPIC) [1]. Here, light is confined within Silicon (Si) structures surrounded by a cladding of Silicon Dioxide (SiO_2). The high core-cladding refractive index difference results in a stronger confinement of light within Silicon and hence, more compact devices [2]. However, its implicit birefringence induces significantly different effective refractive indices for modes propagating through a device [3]. This increases polarization sensitivity, and requires that SiP-based structures be designed separately of each mode, polarization, or telecom wavelength band. As a result, there is a growing need for reliable devices that can perform polarization conversion [4], splitting, and filtering, in order to incorporate polarization diversity in nanophotonic circuits.

Regarding the filtering or splitting of polarizations within a SiP circuit, a passive optical structure is typically used [2], which utilizes the dispersion equation to discriminate between modes in a SiP structure, and spatially separate them so they may then be collected. Such a device, called a polarization beam splitter (PBS) is typically designed to separate the fundamental transverse electric (TE) and transverse magnetic (TM) modes. PBS designs have been extensively explored through the utilization of various concepts in optics such as directional couplers [5], silicon nitride [6], plasmonics [7], sub-wavelength gratings [8], photonic band engineering [9], and multimode interference (MMI) devices [10][11][12]. Directional coupler-based designs require a precise separation between waveguides and are therefore sensitive to variability introduced through the nanofabrication process. Similarly, using alternative materials in augmented low index guiding or plasmonic structures increases fabrication complexity as it normally requires additional post-processing steps. Alternatively, passive Si MMI-based PBS devices are advantageous due to their geometric simplicity and utilization of a single Si core material, which enables a straightforward fabrication process and high tolerance to fabrication nonuniformity. The trade-off with a geometrically stable device, however, is size. MMIs are often limited by their device footprint [13], especially when considering their simplistic functionality as compared to other SiP devices, and the continuous increase of SiEPIC density.

This paper characterizes the response of a novel fabrication tolerant MMI-based polarization beam splitter (PBS) for the C-band wavelength range, over different waveguide input/output configurations. Section I describes the problem space and explains the demand for such a device within the SiP platform.

Excerpt from the Proceedings of the 2017 COMSOL Conference in Boston

Section II explains the device design and concept, as well as the theory necessary to understand MMI structures. Section III translates the design to numerical simulation and describes the utilization of COMSOL Multiphysics in realizing the optical response of such a device structure. Section IV characterizes and optimizes specific parameters regarding the device in order to maximize isolation between TE and TM at their respective outputs. Observations and results are discussed in section VIV along with recommendations for performance improvement and experimental verification. Finally, section VI concludes this report with an optimal parameters and corresponding device performance. References can be found in section VII and acknowledgements in section VIII.

II. Theory

A single mode waveguide limits its spatial dimensions so that the waveguide is able to confine only the fundamental mode. The dimensions can be calculated from the dispersion equation [14], which predicts the effective index dependence on a specific cross-sectional parameter i.e. either height or width, keeping the other constant. The larger the dimensions, the more modes a waveguide is able to support. However, a larger waveguide is also susceptible to interference between the lower and higher order modes as shown in Figure 1.

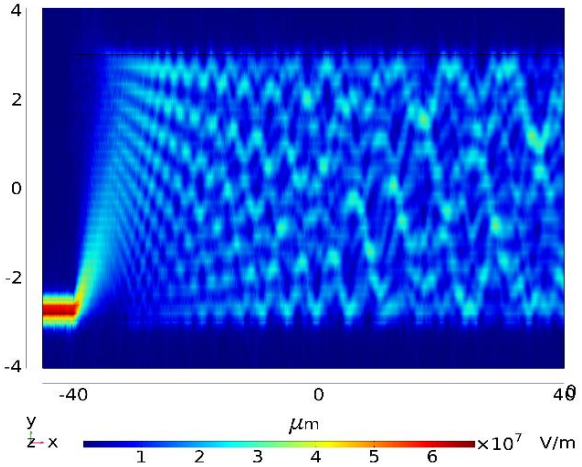

Figure 1: COMSOL simulation showing coupling from a 0.5μm waveguide to a 6μm Si waveguide with 220nm thickness. As light is dispersed through the wider waveguide, energy couples into higher order modes resulting in a periodic interference pattern.

This multimode interference pattern is inherently periodic as can be determined using the guided-mode propagation analysis technique [15] modified for a step-index waveguide that is multimode in the lateral dimension. Using this technique, the self-imaging length for the two lowest order modes can be calculated from the beat length L_π such that [16],

$$L_\pi \approx \frac{4n_r W_e^2}{3\lambda_0} \quad (1)$$

At intervals of this length, the interference pattern resulting from a multimode waveguide is repeated or mirrored, and can hence be collected using an output waveguide that couples out of the structure. However, there is an additional factor; light entering a multimode waveguide experiences modal dispersion [17] due to the differential in effective refractive index for every mode propagating through the waveguide. Additionally, the birefringence in an Si waveguide causes the TE and TM modes in a waveguide to propagate at different phase velocities. This behavior is exploited by collecting light differentially at the output using two separate waveguides – one for TE and one for TM. This enables the design of a passive, all-optical multi-mode interference (MMI)-based polarization beam splitter (PBS).

III. Numerical Simulation Set-Up

The proposed design makes use of an MMI structure to split polarizations. The device is designed for a standard 220nm Si wafer. It can be fabricated via electron beam or UV lithography, and is therefore CMOS compatible. The input waveguide is tapered into a wider waveguide that acts as the MMI. Although both fundamental TE and TM polarizations undergo the same MMI effect, the difference in effective index results in a different L_π for each. Hence, the two output waveguides are used to selectively collect light from each polarization with minimal crosstalk.

As equation (1) implies, the beat length L_π is directly proportional to the effective width of the MMI. In order to minimize the device footprint, a narrower width MMI can significantly reduce the length necessary for self-imaging. However, there is a trade-off regarding using progressively smaller dimensions. They are more susceptible to ± 10nm fabrication variations [2] as it constitutes an increasingly larger proportion of the device.

The position and angle of the input waveguide relative to the MMI-PBS also plays a crucial role in the multimode interference pattern generated within the device. The effective width can also be manipulated by adjusting the angle of the input waveguide. The disadvantage of this method is possible leakage due to the improper confinement of light within the interface between the input waveguide

and MMI. This issue can be solved by tapering the top left corner of the MMI so as to guide light towards the core. Considering image mirroring in MMIs, the bottom right corner is also tapered to focus light towards the output TE port. This results in the parallelogrammatic shape seen in Figure 2.

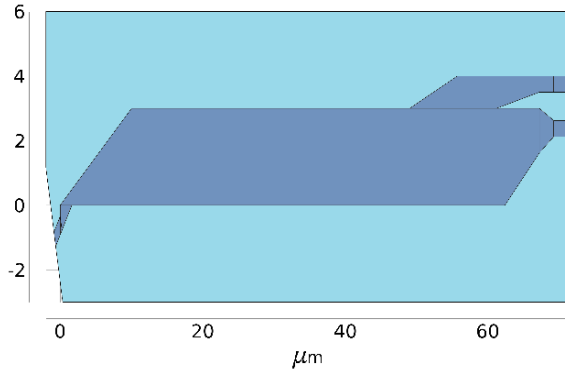

Figure 2: Device geometry of the multi-mode interference - based polarization beam splitter.

The COMSOL simulation environment is used to characterize the optical response of the device geometry for multiple modes and both polarizations. For this purpose, the Wave Optics > Electromagnetic Wave Beam Envelope module was extensively used. Since the system is time independent, it can be solved in the frequency domain. The beam envelope method is found to significantly decrease computation time when working in the frequency domain. This is beneficial to SiP devices as the footprint is typically several orders of magnitude larger than the wavelength, resulting in an otherwise resource heavy computation.

A scattering boundary condition surrounding the simulation region was used to effectively model an infinitely large glass cladding within the spatially finite simulation set-up. The scattering boundary condition assumes that any scattered waves within the cladding will continue to die out at the same rate. A matched boundary condition was used at the port to simulate a perfect wave output. A third important aspect in minimizing computational intensity is mesh optimization. In areas of the structure where detailed calculations are unnecessary, such as the cladding region, a larger mesh size drastically decreases computational intensity with a negligible loss in accuracy.

The optimization of the angle and offset of input waveguide was carried out by assigning a figure of merit for the clarity of the interference pattern that is based on the contrast ratio of the interference image observed. This is directly relevant to the efficiency of separation and collection of TE and TM polarizations.

IV. Characterization and Optimization of Device Geometry

The performance metrics of the device are considered to be the overall insertion loss at each port for the desired polarization. An ideal PBS will therefore have an insertion loss of 0 dB for TM polarized light at the TM port, and 0 dB for TE light at the TE port. The insertion loss at an output waveguide is calculated as a surface integral of the output power flow over the waveguide. This metric is used to sweep device parameters and determine the optimum values for the MMI-PBS within a 3μm effective width.

a. Port Optimization: TM

As the TM interference pattern has a shorter self-imaging length than the pattern corresponding to TE, the TM output is optimized first. This ensures that TM is optimally coupled, and hence implies minimal TM crosstalk at the TE port. TE crosstalk at the TM port has also been considered during this process.

The longitudinal position of the TM port along the X-axis is characterized by sweeping its X position (noted as x_{TM} in Figure 3) at the central wavelength. As expected from considering the interference profile, the insertion loss (IL) for TM light at the TM port is approximately Gaussian-shaped as coupling increases closer to the optimal length. The flatness of the Gaussian appears as a plateau, indicating that the output waveguide is larger than the focus of the MMI pattern, which ensures that the evanescent part of the beam will also be coupled to the TM output. The optimal position appears to be at 60.7μm where the TM power at the TM port reaches a maximum and the crosstalk is at a local minimum.

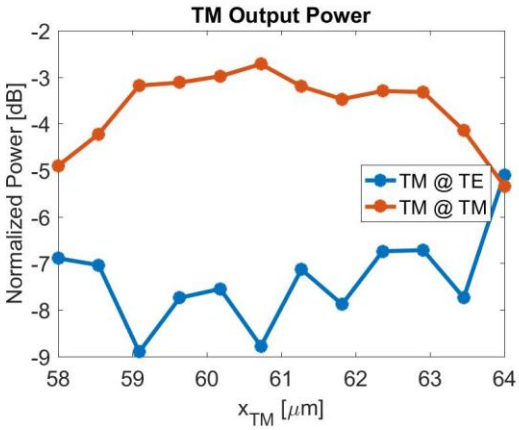

Figure 3: Optimization of TM output for horizontal (x) position of TM output port.

The geometry of the periscopic feature at the TM output port is optimized using the same method. As the

width at the mouth of the periscope (denoted dx_{TM} in Figure 4) is increased, more TM light is directed out from the main MMI structure. The best range of values indicate where the TM output is stable and maximized. Notice from Figure 4 that TE crosstalk encounters a minimum around 6.75μm which further confirms the design parameter.

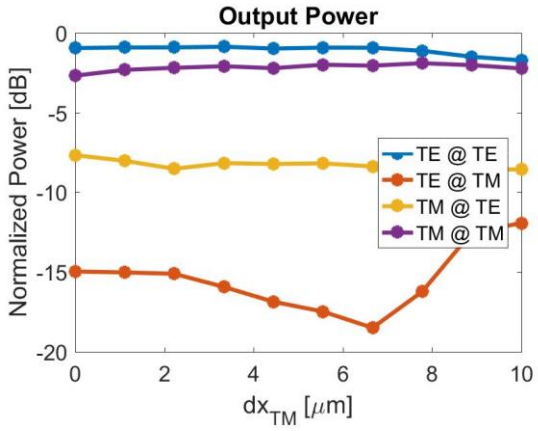

Figure 4: Optimization of TM output for the bottom left periscope feature.

While single variable sweeps are effective at exploring the problem space, certain variables are coupled. In the case of the TM output optimization, as alluded to earlier, the power output at the port is a function of the width of the periscope opening, w_{pl}, and its longitudinal position along the length of the MMI, x_{TM}. This interdependency of variables is represented in Figure 5 where the power at the output for TE and TM are plotted against the two variables being analyzed. At the TM port, the aim is to maximize TM while minimizing TE polarized light.

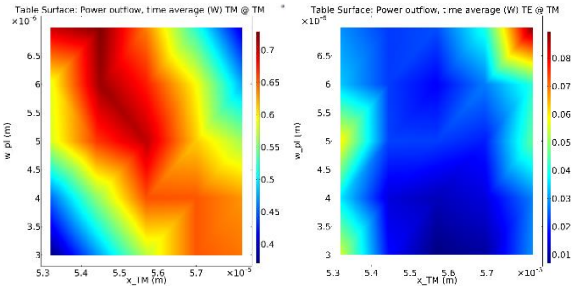

Figure 5: TM port optimization for TM (left) and TE (right) as functions of the X position and width of the TM output.

The TM output is maximized in the top-left region of the plot, whereas TE crosstalk is minimized in the bottom. This necessitates a design choice to be made, in that the center region of the heat map was selected as a compromise between both objectives. This demonstrates the fact that the two objectives for the TM port do not necessarily have a common optimum.

b. Port Optimization: TE

Once the TM output has been optimized, and considering negligible TE crosstalk at the TM port, the TE imaging length can be realized just beyond the TM optimal length. Important parameters that require optimization for TE output are the length of the PBS and the Y position of the TE port (labelled $l_{pbs\ top}$ and y_{TE}, respectively, in Figure 6 and Figure 7). Both sweeps are primarily focused on the TE port; their consequent effect at the TM port is negligible considering the direction of propagation.

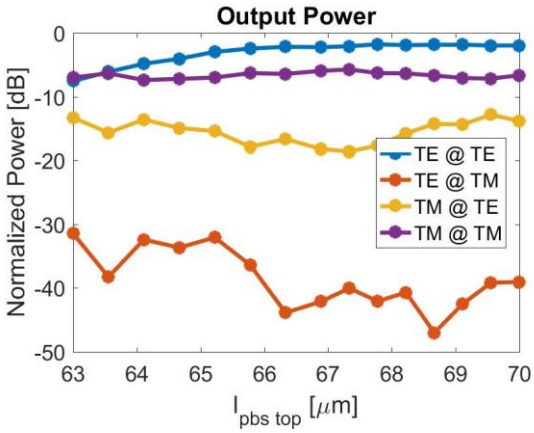

Figure 6: Optimization of TE output over device length.

Increasing the length of the device shows that the TE output power plateaus with a longer flat region than the TM output in Figure 3. This can be attributed to the fact that the TE output is in the direction of propagation of light whereas, the TM output uses band engineering to pull light from the MMI towards the periscopic output. The obvious design choice in this scenario is to minimize size constraints, hence, the smallest length at which TE is maximized.

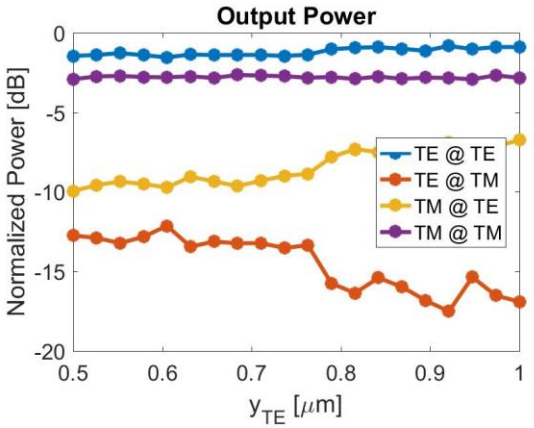

Figure 7: Optimization of TE output for vertical (y) position of TE output port.

Given MMI tapering and optimized device length, the TE output with respect to the lateral (Y) position of the TE port appears to be relatively insensitive to variations. The TM intensity however, increases beyond 0.75µm, which therefore marks the upper limit for possible optimization of the TE output isolation.

Again, as device length and lateral TE output position are coupled parameters, the TE port in Figure 2 is plotted over both length and height. Here, the TE mode propagation is maximized while the TM is minimized. Contrary to the compromise made regarding the TM output optimization, for the TE heatmap, the maximum TE point was chosen. This is because TE is better confined in SiP waveguides than TM (due to the 220nm Si layer thickness), and hence, the TM crosstalk can later be leaked out of the system via a relatively sharp waveguide bend.

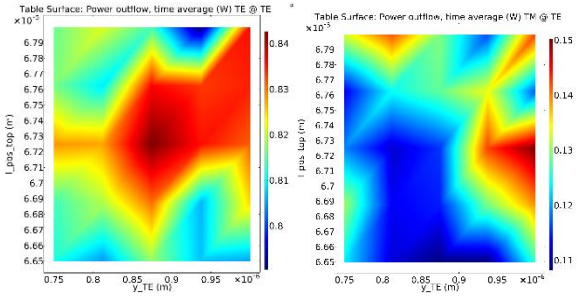

Figure 8: TE port optimization for TE (left) and TM (right).

V. Simulation Results and Observations

The geometry given in Figure 2 is a result of the optimization process carried out through the finite element method in COMSOL Multiphysics software. A similar process was carried out using Lumerical Finite Difference Time Domain software in order to verify the accuracy of results in between either software and method. It was found that the simulations complemented each other, and the results agreed within a 15% tolerance. The MMI pattern propagating through the optimized PBS is shown in Figure 9 for TE and Figure 10 for TM polarized light.

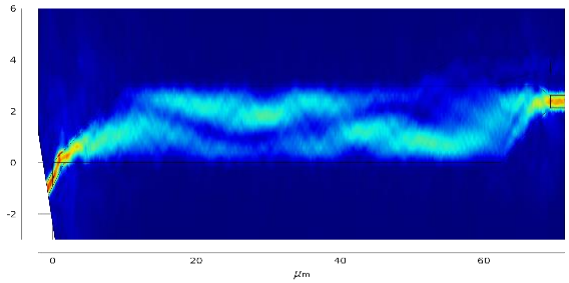

Figure 9: MMI pattern in the PBS as represented by the TE E-Field norm for TE polarized light. Back reflections contribute to the noise in the pattern of the image.

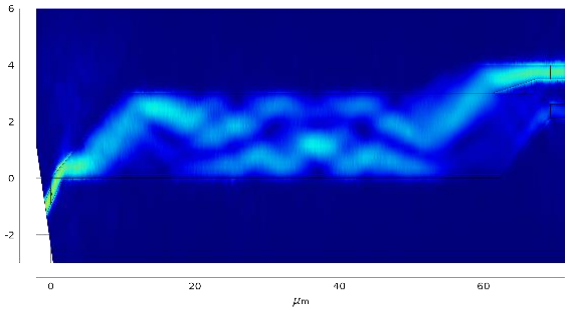

Figure 10: MMI pattern in the PBS as represented by the TM E-Field norm for TM polarized light.

The MMI-PBS has a length of 67µm and a width of 3µm. The transmission spectrum across the C-band range is plotted in Figure 11 for a 100nm optical bandwidth (wider than the telecom C-band) and with a central wavelength of 1550 nm. The TE insertion loss is 0.82 dB with 8.81 dB of TM crosstalk and the TM insertion loss is 1.56 dB with 18.75 dB of TE crosstalk.

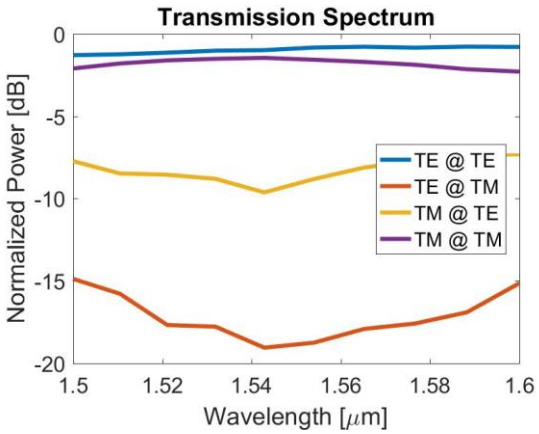

Figure 11: Transmission spectrum of the MMI-PBS for the C-band wavelength range centered at 1.55µm.

VI. Conclusion

We have designed and simulated a compact MMI-based PBS by exploiting new geometric constraints. The device geometry is intentionally designed to be relatively simplistic to ensure its tolerance to fabrication. The simulation can be further expanded by incorporating manufacturing variability through Monte Carlo simulations. The device has a footprint of approximately 200µm^2 with TE isolation of 7.99 dB and a TM isolation of 17.19 dB. Once fabricated, the experimental characterization can be compared with the optical response.

VII. References

[1] Thomson, David, et al. "Roadmap on silicon photonics." Journal of Optics 18, no. 7, 073003 (2016).

[2] Chrostowski, Lukas, and Michael Hochberg. *Silicon photonics design: from devices to systems*. Cambridge University Press (2015).

[3] Caspers, J. Niklas, et al. "Active polarization independent coupling to silicon photonics circuit." *SPIE Photonics Europe*. International Society for Optics and Photonics (2014).

[4] Sacher, Wesley D., et al. "Polarization rotator-splitters in standard active silicon photonics platforms." *Optics express* 22.4, 3777-3786 (2014).

[5] D. Dai, "Silicon Polarization Beam Splitter Based on an Asymmetrical Evanescent Coupling System With Three Optical Waveguides", Journal of Lightwave Technology, vol. 30, no. 20, pp. 3281-3287 (2012).

[6] X. Sun, M. Alam, J. Aitchison and M. Mojahedi, "Compact and broadband polarization beam splitter based on a silicon nitride augmented low-index guiding structure", Optics Letters, vol. 41, no. 1, p. 163 (2015).

[7] B. Bai, Q. Deng and Z. Zhou, "Plasmonic-Assisted Polarization Beam Splitter Based on Bent Directional Coupling", IEEE Photonics Technology Letters, vol. 29, no. 7, pp. 599-602 (2017).

[8] Xu, Yin, and Jinbiao Xiao. "Ultracompact and high efficient silicon-based polarization splitter-rotator using a partially-etched subwavelength grating coupler." *Scientific reports* 6, 27949 (2016).

[9] Shen, Bing, et al. "An integrated-nanophotonics polarization beamsplitter with 2.4× 2.4 μm2 footprint." *Nature Photonics* 9.6, 378-382 (2015).

[10] E. El-Fiky et al.,"A High Extinction Ration, Broadband, and Compact Polarization Beam Splitter Enabled by Cascaded MMIs on Silicon-on-Insulator," Dept. Elect. Eng., McGill Univ., Montreal, Canada (2016).

[11] W. Yang, Y. Xu, Y. Li, X. Wang and Z. Wang, "A compact and wide-band polarization beam splitter based on wedge-shaped MMI coupler in silicon-on-insulator", in Optical Fiber Communications Conference and Exhibition, Los Angeles, CA, USA (2015).

[12] M. Yin, W. Yang, Y. Li, X. Wang and H. Li, "CMOS-compatible and fabrication-tolerant MMI-based polarization beam splitter", Optics Communications, vol. 335, pp. 48-52 (2015).

[13] Y. Jiao, D. Dai, Y. Shi and S. He, "Shortened Polarization Beam Splitters With Two Cascaded Multimode Interference Sections", IEEE Photonics Technology Letters, vol. 21, no. 20, pp. 1538-1540 (2009).

[14] Chen, Chin-Lin. *Foundations for guided-wave optics*. John Wiley & Sons (2006).

[15] Ulrich, R. "Light-propagation and imaging in planar optical waveguides." *Nouvelle Revue d'Optique* 6.5c, 253 (2015).

[16] L. B. Soldano and E. Pennings, "Optical multi-mode interference devices based on self-imaging: principles and applications," Journal of Lightwave Technology 13, 615–627 (1995).

[17] Reed, Graham T., and Andrew P. Knights. *Silicon photonics: an introduction*. John Wiley & Sons (2004).

VIII. Acknowledgements

The authors would like to acknowledge the NSERC Canada Graduate Scholarships and NSERC CREATE Silicon Electronic-Photonic Integrated Circuits (SiEPIC) programs for funding and access to educational material. Software and physical resources were obtained with support from the Canadian Microelectronics Corporation (CMC) and McGill University.